nature nanotechnology

LETTERS

PUBLISHED ONLINE: 4 DECEMBER 2011 | DOI: 10.1038/NNANO.2011.212

Mechanically controlled molecular orbital alignment in single molecule junctions

Christopher Bruot[1], Joshua Hihath[1,2] and Nongjian Tao[1]*

Research in molecular electronics often involves the demonstration of devices that are analogous to conventional semiconductor devices, such as transistors and diodes[1], but it is also possible to perform experiments that have no parallels in conventional electronics. For example, by applying a mechanical force to a molecule bridged between two electrodes, a device known as a molecular junction, it is possible to exploit the interplay between the electrical and mechanical properties of the molecule to control charge transport through the junction[2–8]. 1,4′-Benzenedithiol is the most widely studied molecule in molecular electronics[9–18], and it was shown recently that the molecular orbitals can be gated by an applied electric field[11]. Here, we report how the electromechanical properties of a 1,4′-benzenedithiol molecular junction change as the junction is stretched and compressed. Counterintuitively, the conductance increases by more than an order of magnitude during stretching, and then decreases again as the junction is compressed. Based on simultaneously recorded current–voltage and conductance–voltage characteristics, and inelastic electron tunnelling spectroscopy, we attribute this finding to a strain-induced shift of the highest occupied molecular orbital towards the Fermi level of the electrodes, leading to a resonant enhancement of the conductance. These results, which are in agreement with the predictions of theoretical models[14–17,19,20], also clarify the origins of the long-standing discrepancy between the calculated and measured conductance values of 1,4′-benzenedithiol, which often differ by orders of magnitude[21].

We have studied the charge transport properties of gold–1,4′-benzenedithiol (BDT)–gold junctions using the scanning tunnelling microscopy (STM) break-junction technique[22] in high-vacuum conditions at temperatures between 4 K and 300 K. Break-junction techniques (both STM and a related approach based on a mechanically controlled break junction) have been widely used to create and study electron transport in molecules[4,23]. To determine the conductance of a single BDT molecular junction, we first performed repeated break-junction cycles, where one electrode is brought into contact with the other and pulled back while the current is recorded (Fig. 1a). If a molecular junction is formed during the stretching process, steps appear in the current versus distance trace, and by repeating this procedure thousands of times it is possible to determine the most likely conductance of a single molecule based on statistical analysis[24]. The conductance histograms (Fig. 1b) show broad peaks near $0.01G_0$ (where $G_0 = 2e^2/h$), which agree with previous studies by various groups[9,11–13]. Details of the histogram distribution are discussed in the Supplementary Information.

At low temperatures, plots of conductance versus electrode displacement often show an increase in molecular conductance during stretching. We define displacement here as the relative movement of the two electrodes, and define zero displacement as the point where the conductance drops from G_0 to the tunnelling regime for each trace. Some of the junctions yield an increase of more than one order of magnitude in the conductance upon stretching, raising the conductance to a few tenths of $1G_0$ before breakdown (Fig. 1c,d). Additionally, many of the conductance traces show a small decrease in conductance before increasing. In total, at low temperature, ~70% of the conductance versus distance traces have a plateau region with an increase in the conductance. The conductance measured at the last stage of stretching is close to the value of conductance for BDT calculated using theoretical models[21].

The large increase in conductance is counterintuitive, because increasing the distance between the two electrodes is expected to weaken molecule–electrode coupling and increase tunnelling distance, which one would expect to lead to a decrease in conductance rather than an increase. This observation has been made for alkanedithiol junctions[7,25,26]. We believe that the increase in conductance is a result of force-induced resonant tunnelling, an effect that occurs when the weakening of the molecule–electrode coupling causes a shift in molecular energy level closer to the electrode Fermi level[14–17]. Theoretical studies[17] predict that changing either of the molecule–electrode contacts in a molecular junction can significantly affect the alignment of the molecular energy levels relative to the electrode Fermi levels, and thus change the conductance. In the case of a BDT junction, it has been shown that its highest occupied molecular orbital (HOMO)-related states are located far below the Fermi level in the relaxed configuration[20,27]. However, on stretching the molecular junction, electronic coupling between the molecule and electrodes decreases, and the HOMO-related states move up towards the Fermi level, leading to resonant tunnelling. Therefore, even though the electrodes are being separated during the stretching process, this shift in the HOMO level causes a substantial increase in the conductance upon stretching because it causes a decrease in the tunnelling energy barrier. Several other theoretical studies have been performed to elucidate the conductance behaviour of BDT[14–16]. Although the conductance values calculated using different theories vary over a large range, the prediction that the value increases with stretching is robust and insensitive to the details of the different models[14–16,19,20].

To better understand the evolution of the conductance increase under stretching conditions we created many molecular junctions and studied the current–voltage (I–V), conductance–voltage (G–V) and inelastic electron tunnelling spectroscopy (IETS) characteristics while gradually stretching and compressing the junctions[28]. Figure 2 shows an example of one junction in which the I–V, G–V and IETS curves were recorded while the electrode displacement was changed in ~0.01 nm increments. After the junction was formed (region I in Fig. 2a), an initial increase in conductance was noticed as the electrodes were separated by a small distance (region II). To avoid breaking the junction and to explore the

[1]Center for Bioelectronics and Biosensors, Biodesign Institute, School of Electrical, Energy and Computer Engineering, Arizona State University; Tempe, Arizona 85287-5801, USA, [2]Department of Electrical and Computer Engineering, University of California Davis, Davis, California 95616, USA.
*e-mail: njtao@asu.edu

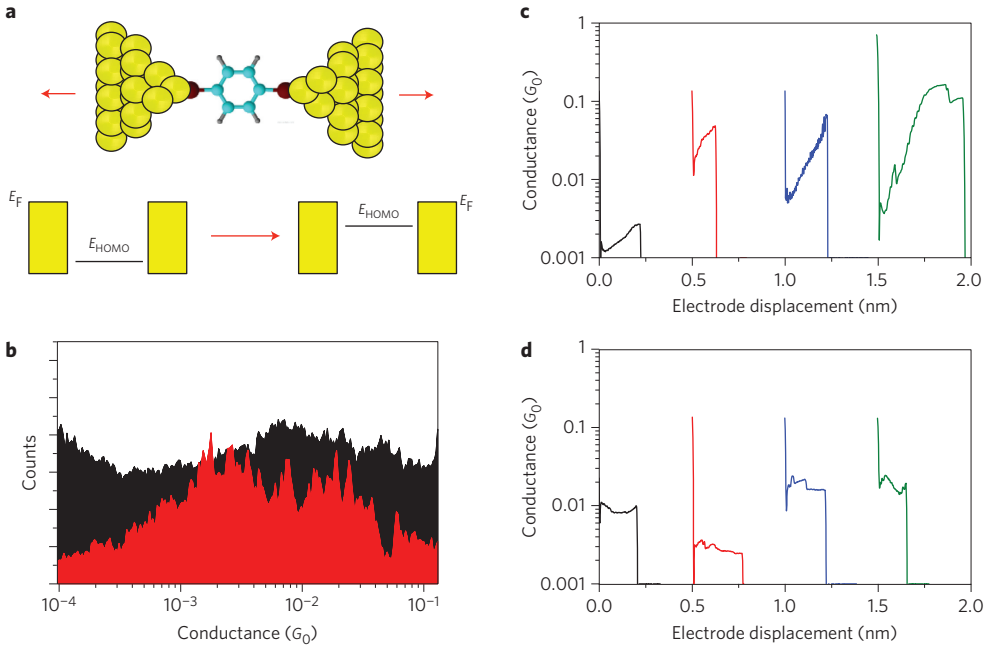

Figure 1 | Changes in conductance of BDT due to stretching. a, Schematic of a molecular junction (top). Schematic energy diagram (bottom) showing how the energy of the HOMO changes relative to E_F of the electrodes as electrode separation increases. **b**, Characteristic conductance histograms at room temperature (black) and 4.2 K (red). Histograms offset for clarity. **c**,**d**, Plots of conductance (in units of G_0) versus electrode displacement measured at 4.2 K. For some junctions the conductance increases with displacement (**c**), whereas for others the conductance–displacement curves are either flat or bowl-shaped (**d**). Different colours in **c** and **d** represent different junctions, and the traces have been offset for clarity.

reversibility of this feature, the direction of movement was then reversed, and electrode displacement was decreased (region III, shown in blue). The separation of the electrodes was then increased again (region IV, shown in black) to ensure the reproducibility of the conductance behaviour. The 'bowl'-shaped conductance behaviour shown in Fig. 2a is characteristic of the force-induced resonance predicted by theory[20,27]. It suggests that when the junction is compressed the BDT molecule is tilted between the electrodes, which causes an increase in conductance due to lateral π-electron coupling between the molecule and electrodes[7,25]. When the junction is stretched, however, electronic coupling between the molecule and electrodes is reduced, causing a shift in the HOMO level towards the Fermi energy of the electrodes, and a corresponding increase in conductance. The change in conductance is fully reversible, and the force-induced increase in conductance is apparent in the initial stretching (region II) and extends even further after the retrace is completed (region IV).

We also recorded both the conductance G and the inelastic electron tunnelling (IET) as a function of bias voltage V at several different displacements during the compression and extension cycles. The G–V spectra reveal significant, continuous and fully reversible changes during the compression and extension cycles. When the junction is extended (positions 1 and 8 in Fig. 2a,b), the G–V curve is highly asymmetric, but this asymmetry decreases as the displacement decreases (Fig. 2d). Because the molecule is symmetric, the asymmetry in the G–V curves must be due to asymmetric contacts formed between the molecule and the two gold electrodes. The two contacts are in series, so one expects that the weaker of the two will be stretched more, which leads to even more asymmetry in the contacts, and explains the increase in asymmetry with electrode separation.

The most obvious change in the IET spectra during the stretching and compressing cycle is the change in the vibration mode at ±14 mV (Fig. 2c). The amplitudes of this low-frequency mode change continuously with displacement, becoming asymmetric as the junction is extended and more symmetric as the junction is compressed (Fig. 2e). This mode could be due to either the collective motion of BDT with respect to the gold electrodes[29,30] or to gold–gold bonds in the contact[31]. The observed change in the ±14 mV mode demonstrates that a strain is being applied to the molecular junction, and that the stretching/compression takes place primarily at the molecule–electrode contact. As is predicted theoretically[14–17], this change in the contact decreases the coupling between the molecule and the electrode, and shifts the HOMO level towards the electrode Fermi level, causing an increase in molecular conductance. Although there is a systematic change in the peak amplitude, the change in the peak frequency (position) is less obvious because it is relatively small and may be obfuscated by the peak width in most cases[8,32]. However, obvious changes in peak frequency have also been observed in some junctions (for example, the mode around 40 mV in Fig. 3d).

The conductance, symmetry of the G–V curves and low-frequency vibration mode in the IET spectrum all change continuously and reversibly upon repeated stretching and compressing of the molecular junction. These observations indicate that the increase in G at the end of the stretching cycle is not due to large and abrupt changes in the molecule–electrode contact geometry, as is seen in other systems[33], but is instead due to a gradual and reversible stretching of the bond at the contacts. Large abrupt atomic rearrangements at the contacts can also be observed, which is, however, much different from the continuous changes discussed above. Figure 3 shows two BDT junctions undergoing abrupt configuration changes during stretching. The first junction showed a clear plateau, and the stretching process was stopped at position 1 to begin recording the I–V, G–V and IETS characteristics (Fig. 3a–d). Upon further stretching of the junction a clear and gradual increase in conductance is observed, together with an increase in the asymmetry of the G–V curve. However, when the junction is stretched to a distance of ~0.23 nm, close to the size of a gold atom, the conductance drops abruptly to a value below the initial conductance at

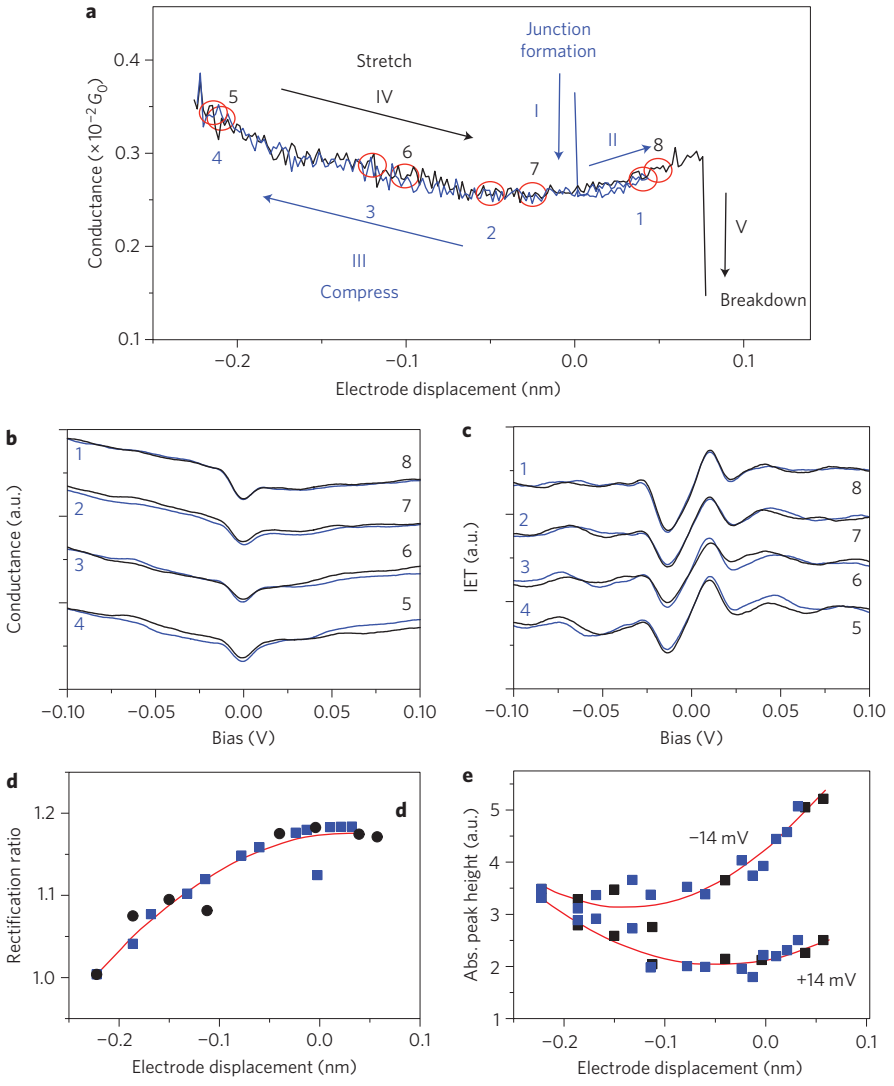

Figure 2 | Differential conductance and IETS of BDT junctions as a result of stretching and compressing. a, Plot of conductance *G* versus electrode displacement for a junction during repeated stretching and compressing at 4.2 K. **b**, Differential conductance curves (*G* versus *V*) for positions 1–8 in **a**. The curves show clear, reversible changes in asymmetry as the mechanical force changes. **c**, IET spectra (d^2I/dV^2 versus *V*) also show reversible changes. Both the *G*–*V* curves and the IET spectra are offset for clarity. **d**,**e**, Plots of rectification ratio at $V = 0.2$ V (**d**) and peak height ratio for the ±14 mV mode (**e**) versus electrode displacement. Red curves are fits to guide the eye. See Supplementary Information for all *G*–*V* curves and IET spectra for this junction, including the assignment of vibration modes to the observed peaks.

position 1. This sudden change in conductance is also accompanied by a sudden change in the symmetry of the *G*–*V* curves. Upon further stretching the conductance, the asymmetry increases again for a similar distance of ∼0.23 nm before the junction finally breaks down.

There is also a sudden switch[34] in the conductance of the second junction at a displacement of 0.14 nm (Fig. 3e). The conductance increases upon further stretching until breakdown when the junction is stretched to ∼0.27 nm. Again, the *G*–*V* curves show large and abrupt changes associated with the switch (Fig. 3f). These data further confirm that the continuous changes in the conductance, *G*–*V* curves and IET spectra shown in Fig. 2 are due to continuous stretching in the molecule–electrode contacts rather than any sudden changes in the geometry.

The IET spectra for the first junction show a large increase in the peak amplitude and a change in the line shape of the modes between 0.1 and 0.2 V as the junction elongates and conductance increases (Fig. 3c,d). These modes are due to benzene ring vibrations (Supplementary Table S1). Although this change in the IETS peaks could be caused by other factors, such as dipole coupling[35], it is consistent with the theory of IETS peaks near resonance, which predicts an increase in the amplitude and the development of a derivative-like feature[11,36,37]. This resonant enhancement may also explain the systematic increase in the IETS peak amplitude shown in Fig. 2. A much larger increase in the IETS peaks is shown in Supplementary Fig. S5, where the transport is brought closer to resonance upon stretching than the junctions shown in Figs 2 and 3.

So far, we have demonstrated that conductance can increase with stretching of a BDT junction. When this increase occurs, it is accompanied by a continuous increase in the asymmetry of the *G*–*V* curves, a change in amplitude of the low-frequency vibration mode, and a change in the IETS peak amplitude and line shape. These points demonstrate that the conductance increase is due to continuous stretching in the molecule–electrode contact, and support the model of a force-induced shift in the molecular orbital. However, to fully demonstrate the emergence of a resonant tunnelling feature during elongation, it is also important to show

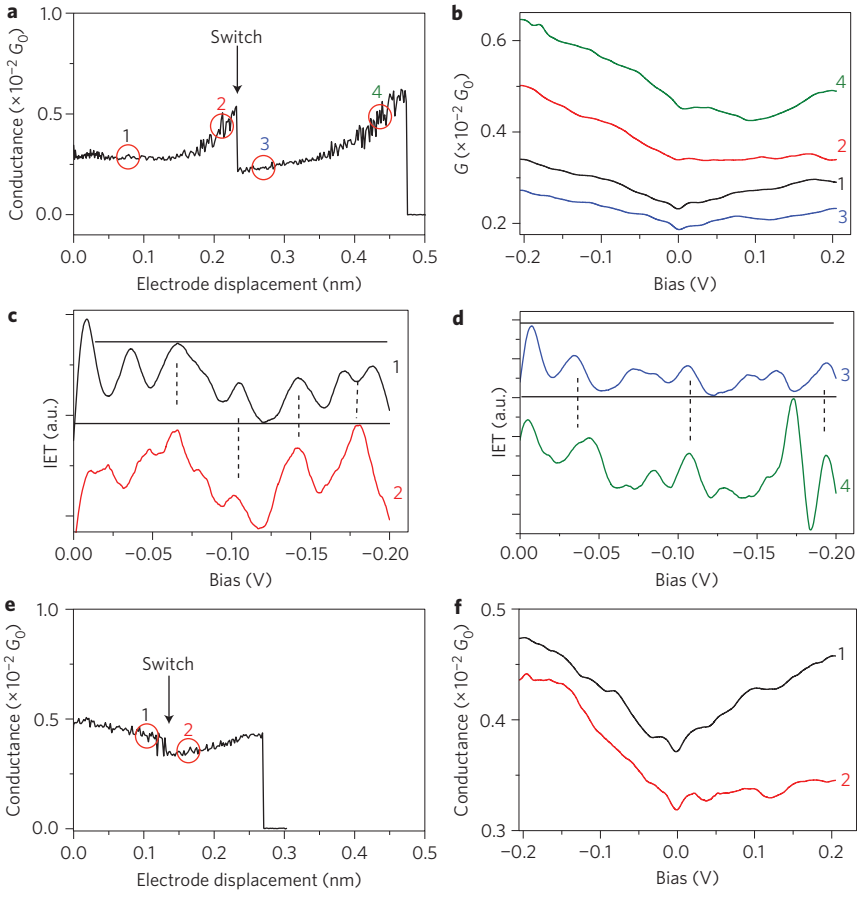

Figure 3 | Conductance switching behaviour of two BDT junctions. a, Plot of conductance *G* versus electrode displacement showing switching and increasing conductance behaviour. **b**, Differential conductance (*G*–*V*) curves at the four different positions indicated in **a**: the curve at position 3 is clearly more symmetric than at position 2. **c**,**d**, IET spectra at positions 1 and 2 (**c**) and 3 and 4 (**d**) in **a**, showing that changes in the conductance lead to changes in the intensity and shape of the peaks. IET spectra are plotted on the same scale and are offset for clarity. **e**, Plot of conductance versus displacement for a different junction, showing the conductance first decreasing and then increasing after a switching event. **f**, *G*–*V* curves from positions 1 and 2 in **e**. All measurements performed at 4.2 K.

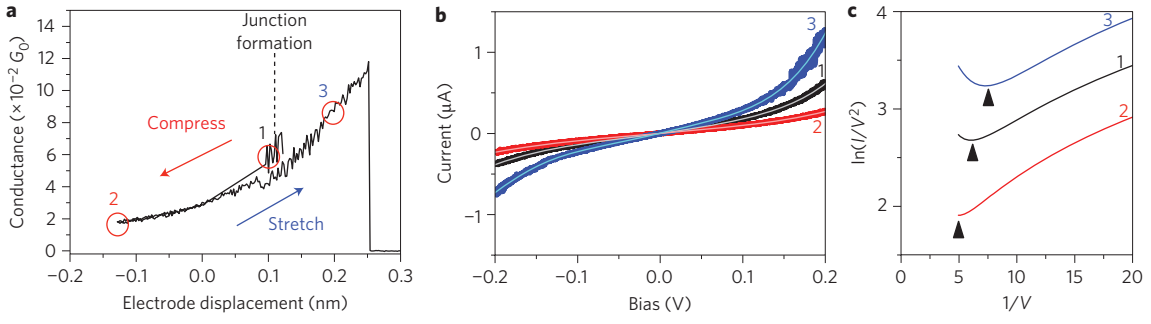

Figure 4 | Exploring the energy levels of a molecular junction. a, Plot of conductance versus electrode displacement of a BDT junction at 4.2 K recorded with the junction being stretched and compressed much faster than the plots shown in Figs 2 and 3. The conductance decreases when the junction is compressed, and then increases to a relatively high value when the junction is stretched. **b**, Plots of current *I* versus bias voltage *V* at the three positions indicated in **a**, recorded with *V* being swept much faster than the plots shown in Figs 2 and 3. Thin lines are fits to the data. **c**, Plots of $\ln(I/V^2)$ versus $1/V$ for three different values of the displacement (based on fits to the *I*–*V* curves in **b**). The height of the barrier that electrons have to tunnel through is determined by the transition voltage, which is the voltage corresponding to the minimum of each plot (indicated by arrows). The height of the barrier decreases as the molecule is stretched.

that the energy levels of the molecular system change upon stretching. To explore this possibility we performed stretching/bias sweep measurements in which the bias was swept quickly and the tip was moved quickly (rather than the slow bias sweeps used to obtain the high-resolution *G*–*V* and IET spectra described above); this allowed the junction to reach much higher conductance values before breakdown (Fig. 4a). Upon stretching, the current increases nonlinearly with bias for higher values of the bias (Fig. 4b), and as the junction

is stretched the increase becomes even more prevalent, indicating a change in the proximity of the energy of the HOMO level to the Fermi energy of the electrodes.

To better demonstrate what happens to the energy levels of the molecule, we use a technique called transition voltage spectroscopy (TVS), which has recently emerged as a robust method for probing the energy levels of molecular devices[11,38–40]. In TVS we plot $\ln(I/V^2)$ as a function of $1/V$, and these plots are expected to have a negative slope for biases above $|\varphi/e|$ and a positive slope below $|\varphi/e|$, so there is a minimum at $V = \varphi/e$, where φ is the barrier height and e is the electron charge. Therefore, if the energy of the HOMO level is moving closer to the Fermi energy during the stretching process, this minimum should shift to lower biases (higher $1/V$). We observe a clear decrease in the TVS minimum with stretching (Fig. 4c), which indicates that the energy difference between the HOMO level and the Fermi level is decreasing, thus moving the system closer to a resonant condition. For large values of the displacement (point 3 in Fig. 4a), the value of the TVS minimum yields a barrier height of ~0.14 eV. This rather low barrier suggests that resonant tunnelling is responsible for a significant amount of electron transport. Additional TVS data are shown in the Supplementary Information.

In conclusion, we have found that the conductance of individual BDT molecules bridged between two gold electrodes can increase by more than an order of magnitude when the molecules are stretched, before breaking down. This counterintuitive observation is attributed to force-induced resonant enhancement, which occurs because the HOMO-related states move towards the Fermi level of the gold electrodes when the molecule–electrode coupling decreases upon stretching. Repeated stretching and compressing can reproduce the increase and decrease of the conductance with no hysteresis, indicating a continuous stretching and relaxation in the bonds at the molecule–electrode contact, rather than an abrupt rearrangement of contact geometry. Furthermore, we have shown that the energy barrier decreases as the junction is stretched. These results, which are in agreement with theoretical calculations, also demonstrate the feasibility of electromechanical devices based on the use of mechanical force to tune electron tunnelling in and out of resonance. Such device functions cannot be created with conventional semiconductor materials.

Methods

Gold substrates were prepared by thermally evaporating 130 nm of gold (Alfa Aesar 99.9999% purity) on a cleaved mica surface (Ted Pella), and then annealing in a hydrogen flame for ~1 min before sample preparation. BDT samples were prepared by submersing the gold substrate in ~1 mM BDT solution in methanol for ~12 h. The substrate was then thoroughly rinsed using methanol, dried with nitrogen gas, and placed in a homebuilt STM with a freshly cut gold tip (99.998% purity, Alfa Aesar). The STM assembly was then placed in a liquid-helium cryostat (Janis Research Company) and placed under a vacuum of 2×10^{-6} torr. The Dewar cryostat was then filled with liquid helium and the STM cooled to ~4.2 K. Once the temperature of the system was stable, the tip of the STM was brought into the proximity of the substrate and the break-junction, I–V and G–V experiments were performed. Break-junction experiments at higher temperatures were performed with no liquid helium in the Dewar once the STM had heated to a stable temperature.

The current measurements for the break-junction and I–V experiments were performed using a simple transconductance amplifier, with a gain of either 100 nA V^{-1} or 1 μA V^{-1}. For I–V, G–V and IETS, after a molecular plateau was detected and the tip was stopped, the voltage was swept at a rate of 0.005 Hz. The tip was then moved, either towards or away from the substrate, in increments of ~0.01 nm until the junction broke down. The G–V curves were obtained using a lock-in amplifier technique with a modulation amplitude of 1 mV, a reference frequency of 23 kHz and a sweep rate of 0.005 Hz. The IET spectra were obtained by taking the numerical derivative of the lock-in output using LabView and Matlab software[28]. Additionally, TVS plots were obtained by fitting the high-bias sweep I–V curve with a seventh-order polynomial and using this fit as the current in the TVS to minimize the effects of noise in the I–V curve.

Received 20 September 2011; accepted 31 October 2011; published online 4 December 2011

References

1. Aviram, A. & Ratner, M. Molecular rectifiers. *Chem. Phys. Lett.* **29,** 277–283 (1974).
2. Joachim, C., Gimzewski, J. K. & Aviram, A. Electronics using hybrid-molecular and mono-molecular devices. *Nature* **408,** 541–548 (2000).
3. Xu, Bingqian *et al.* Electromechanical and conductance switching properties of single oligothiophene molecules. *Nano Lett.* **5,** 1491–1495 (2005).
4. Parks, J. J. *et al.* Mechanical control of spin states in spin-1 molecules and the underscreened Kondo effect. *Science* **328,** 1370–1373 (2010).
5. Meisner, J. S. *et al.* A single-molecule potentiometer. *Nano Lett.* **11,** 1575–1579 (2011).
6. Quek, S. Y. *et al.* Mechanically controlled binary conductance switching of a single-molecule junction. *Nature Nanotech.* **4,** 230–234 (2009).
7. Diez-Perez, I. *et al.* Controlling single molecule conductance through lateral coupling of π-orbitals. *Nature Nanotech.* **6,** 226–231 (2011).
8. Kim, Y. *et al.* Conductance and vibrational states of single-molecule junctions controlled by mechanical stretching and material variation. *Phys. Rev. Lett.* **106,** 196804 (2011).
9. Xiao, X. Y., Xu, B. Q & Tao, N. J. Measurement of single molecule conductance: benzenedithiol and benzenedimethanethiol. *Nano Lett.* **4,** 267–271 (2004).
10. Reed, M. A. *et al.* Conductance of a molecular junction. *Science* **278,** 252–254 (1997).
11. Song, H. *et al.* Observation of molecular orbital gating. *Nature* **462,** 1039–1043 (2009).
12. Tsutsui, M., Teramae, Y., Kurokawa, S. & Sakai, A. High-conductance states of single benzenedithiol molecules. *Appl. Phys. Lett.* **89,** 163111 (2006).
13. Taniguchi, M., Tsutsui, M., Yokota, K. & Kawai, T. Inelastic electron tunneling spectroscopy of single-molecule junctions using a mechanically controllable break junction. *Nanotechnology* **20,** 434008 (2009).
14. Romaner, L. *et al.* Stretching and breaking of a molecular junction. *Small* **2,** 1468–1475 (2006).
15. Ke, S. H., Baranger, H. U. & Yang, W. T. Contact atomic structure and electron transport through molecules. *J. Chem. Phys.* **122,** 074704 (2005).
16. Li, Z. & Kosov, D. S. Nature of well-defined conductance of amine-anchored molecular junctions: density functional calculations. *Phys. Rev. B* **76,** 035415 (2007).
17. Xue, Y. & Ratner, M. A. Microscopic study of electrical transport through individual molecules with metallic contacts. II. Effect of the interface structure. *Phys. Rev. B.* **68,** 115406 (2003).
18. Kim, Y. *et al.* Benzenedithiol: a broad-range single-channel molecular conductor. *Nano Lett.* **11,** 3734–3738 (2011).
19. Toher, C. & Sanvito, S. Efficient atomic self-interaction correction scheme for nonequilibrium quantum transport. *Phys. Rev. Lett.* **99,** 056801 (2007).
20. Pontes, R. B. *et al. Ab initio* calculations of structural evolution and conductance of benzene-1,4-dithiol on gold leads. *ACS Nano* **5,** 795–804 (2011).
21. Lindsay, S. M. & Ratner, M. A. Molecular transport junctions: clearing mists. *Adv. Mater.* **19,** 23–31 (2007).
22. Xu, B. Q. & Tao, N. J. Measurement of single molecule conductance by repeated formation of molecular junctions. *Science* **301,** 1221–1223 (2003).
23. Smit, R. H. M. *et al.* Measurement of the conductance of a hydrogen molecule. *Nature* **419,** 906–909 (2002).
24. Hihath, J. & Tao, N. J. Rapid measurement of single-molecule conductance. *Nanotechnology* **19,** 265204 (2008).
25. Haiss, W. *et al.* Precision control of single-molecule electrical junctions. *Nature Mater.* **5,** 995–1002 (2006).
26. Zhou, J. F. & Xu, B. Q. Determining contact potential barrier effects on electronic transport in single molecular junctions. *Appl. Phys. Lett.* **99,** 042104 (2011).
27. Sergueev, N., Tsetseris, L., Varga, K. & Pantelides, S. Configuration and conductance evolution of benzene–dithiol molecular junctions under elongation. *Phys. Rev. B* **82,** 073106 (2010).
28. Hihath, J., Bruot, C. & Tao, N. J. Electron–phonon interactions in single octanedithiol molecular junctions. *ACS Nano* **4,** 3823–3830 (2010).
29. Luo, Y., Lin, L. L. & Wang, C. K. Inelastic electron tunneling spectroscopy of gold–benzenedithiol–gold junctions: accurate determination of molecular conformation. *ACS Nano* **5,** 2257–2263 (2011).
30. Chen, Y. C., Zwolak, M. & Di Ventra, M. Inelastic current–voltage characteristics of atomic and molecular junctions. *Nano Lett.* **4,** 1709–1712 (2004).
31. Agrait, N., Untiedt, C., Rubio-Bollinger, G. & Vieira, S. Onset of energy dissipation in ballistic atomic wires. *Phys. Rev. Lett.* **88,** 216803 (2002).
32. Arroyo, C. R. *et al.* Characterization of single-molecule pentanedithiol junctions by inelastic electron tunneling spectroscopy and first-principles calculations. *Phys. Rev. B* **81,** 075405 (2010).
33. Kamenetska, M. *et al.* Formation and evolution of single-molecule junctions. *Phys. Rev. Lett.* **102,** 126803 (2009).
34. Taniguchi, M., Tsutsui, M., Yokota, K. & Kawai, T. Mechanically-controllable single molecule switch based on configuration specific electrical conductivity of metal–molecule–metal junctions. *Chem. Sci.* **1,** 247–253 (2010).

35. Okabayashi, N., Konda, Y. & Komeda, T. Inelastic electron tunneling spectroscopy of an alkanethiol self-assembled monolayer using scanning tunneling microscopy. *Phys. Rev. Lett.* **100,** 217801 (2008).
36. Galperin, M., Ratner, M. A. & Nitzan, A. Inelastic electron tunneling spectroscopy in molecular junctions: peaks and dips. *J. Chem. Phys.* **121,** 11965–11979 (2004).
37. Paulsson, M. *et al.* Unified description of inelastic propensity rules for electron transport through nanoscale junctions. *Phys. Rev. Lett.* **100,** 226604 (2008).
38. Beebe, J. M., Kim, B., Frisbie, C. D. & Kushmerick, J. G. Measuring relative barrier heights in molecular electronic junctions with transition voltage spectroscopy. *ACS Nano* **2,** 827–832 (2008).
39. Huisman, E. H., Guedon, C. M., van Wees, B. J. & van der Molen, S. J. Interpretation of transition voltage spectroscopy. *Nano Lett.* **9,** 3909–3913 (2009).
40. Trouwborst, M. L. *et al.* Transition voltage spectroscopy and the nature of vacuum tunneling. *Nano Lett.* **11,** 614–617 (2011).

Acknowledgements

This work was supported by the Basic Energy Science programme of the Department of Energy (DE-FG03-01ER45943, C.B.) and the National Science Foundation (CHE-1105588 and ECS-0925498, J.H. and N.J.T.).

Author contributions

N.J.T. conceived the experiment. C.B. and J.H. performed the experiment and analysed the data. C.B., J.H. and N.J.T. co-wrote the paper.

Additional information

The authors declare no competing financial interests. Supplementary information accompanies this paper at www.nature.com/naturenanotechnology. Reprints and permission information is available online at http://www.nature.com/reprints. Correspondence and requests for materials should be addressed to N.T.